

We are IntechOpen, the world's leading publisher of Open Access books Built by scientists, for scientists

6,900

Open access books available

186,000

International authors and editors

200M

Downloads

Our authors are among the

154

Countries delivered to

TOP 1%

most cited scientists

12.2%

Contributors from top 500 universities



WEB OF SCIENCE™

Selection of our books indexed in the Book Citation Index
in Web of Science™ Core Collection (BKCI)

Interested in publishing with us?
Contact book.department@intechopen.com

Numbers displayed above are based on latest data collected.
For more information visit www.intechopen.com



Optic-Fiber Temperature Sensor

Yundong Zhang, Huaiyin Su, Kai Ma, Fuxing Zhu,
Ying Guo and Weiguo Jiang

Additional information is available at the end of the chapter

<http://dx.doi.org/10.5772/intechopen.74207>

Abstract

As an important parameter in industry, agriculture, biomedical, and aerospace, temperature possesses a significant position for the development of our society. Thus, it has become a hot point to develop novel sensors for temperature monitoring. Compared with traditional electronic sensors, optical fiber sensors break out for the compact structure, corrosion resistance, multiplex and remote sensing capability, cheap prices, and large transmission capacity. Especially the phase modulation type optical fiber sensors attract much attention for the fast and accurate measurement of the external parameters in a large dynamic measurement range. In this work, we review the optical fiber Mach-Zehnder interferometer (MZI) for temperature sensing which is widely used these years. The fundamental principles of MZI fiber sensors are proposed and discussed to further understand MZI. Different kind of structures for temperature sensing of recent years are summarized as several typical MZI categories and their advantages and disadvantages are indicated separately. Finally, we make a conclusion of the MZI temperature sensing and several methods typically to realize the MZI in practical application for the readers.

Keywords: temperature monitoring, optical fiber sensors, Mach-Zehnder interferometer, phase modulation, fast and accurate measurement

1. Introduction

Temperature monitoring means a lot for agriculture, industry, transportation, and many aspects of our society, thus, it is important to develop the sensors for temperature detection. Compared with electronic sensors, optical fiber sensors receive highly attention as soon as it came out for the compact size, high sensitivity, and easy to integrated.

Optical fiber Mach-Zehnder interferometer (MZI) is one of the typical structures which has been widely used for sensing these years. It contains two interferometer arms, called reference arm and probe arm respectively and the two arms are usually connected by couplers. The probe arm will be placed in external environment to be measured in the experiment, the light propagating within the arm will be influenced by the external parameters. Thus, the phase difference of the light in two arms will be changed and the interference fringe will be shifted with it, and the wavelength shift is the final parameter we use mostly for probing the external environment change.

Due to the shortages of the traditional separated MZI structures, recently, the integrative Inline MZI sensor devices obtain more attention and become a hot point for the researchers. The Inline MZI can integrate the beam splitter, beam combination, and interference arms together, and realize the interference function within single fiber which shows plenty of advantages such as: compact structure, small volume, fast response, high sensitivity, and large dynamic range. Thus the Inline MZI research develops significantly in the recent years especially for temperature sensing. In this work, we will introduce the recent research of Inline MZI and its application in temperature monitoring.

The Inline MZI can be divided into several categories according to their materials and fabrication methods, such as special optical fiber MZI, hydrofluoric acid corrosion MZI, MZI with femtosecond laser, abrupt tapered, up-tapered, lateral-offset splicing joint MZI, and so on. All these configurations contain different application situations, therefore, we review these typical Inline MZI and discuss their advantages and disadvantages for the readers. Finally, we make a conclusion of the MZI temperature sensing and give out the possible trends of MZI optical fiber sensors for temperature monitoring in the future development.

1.1. Theory of temperature sensor based on optical fiber MZI

Optical fiber Mach-Zehnder Interferometer (MZI) based on double-beam interference consists of two couples connecting reference arm and probe arm. The input light is divided into two parts by the first coupler, then propagating along the reference arm and probe arm, respectively. When the length difference of the interference arms is far less than the coherent length of incident light, the output lights of two arms arrive at the second coupler and generate a coherent superposition so as to produce interference. **Figure 1** schematically illustrates the diagram of the optical fiber Mach-Zehnder Interferometer.

The incident light field is

$$E_0 = A_0 e^{j(\omega t - k_0 n l)} \quad (1)$$

where A_0 is the amplitude of light; ω is the frequency of transmission; k_0 is the constant of transmission; n is the refractive index of fiber core; l is optical path.

Thus the intensity of incident light is

$$I_0 = E_0 \cdot E_0^* = A_0^2 \quad (2)$$

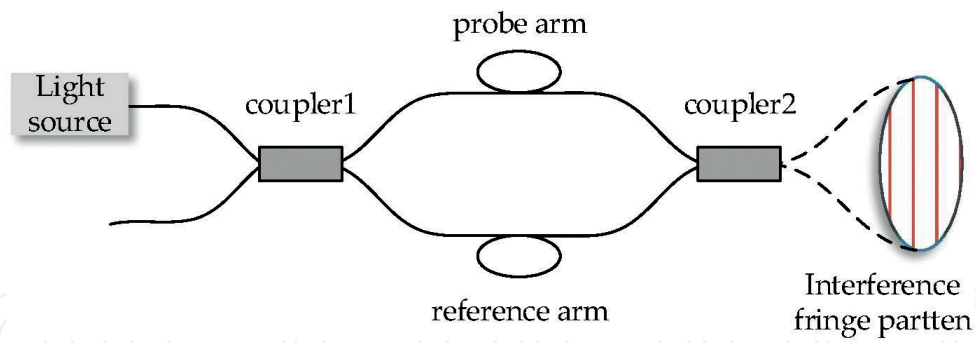


Figure 1. The schematic diagram of optical fiber MZI.

Assuming the coupling coefficients of the two MZI couplers are ε , the phase delay of $\pi/2$ will occur in the probe arm due to the cross-coupling of incident light passing through the first coupler. Before the light arriving at the second coupler, the optical field transmission functions of the reference arms and probe arm can be written as

$$E_{r1} = A_0 \sqrt{\varepsilon} e^{j(\omega t - k_0 n_r l_r)} \quad (3)$$

$$E_{s1} = A_0 \sqrt{1 - \varepsilon} e^{j(\omega t - k_0 n_s l_s + \frac{\pi}{2})} \quad (4)$$

where n_r and n_s are the refractive index, l_r and l_s are the length of reference arm and probe arm, respectively.

The phase delay of $\pi/2$ will occur again when the two lights superpose in the second coupler to generate interference. There are two cases in the following.

(1) The second phase delay of $\pi/2$ appearing again in the probe arm, not in reference arm.

$$E_{r2} = A_0 \sqrt{\varepsilon^2} e^{j(\omega t - k_0 n_r l_r)} \quad (5)$$

$$E_{s2} = A_0 \sqrt{(1 - \varepsilon)^2} e^{j(\omega t - k_0 n_s l_s + \pi)} \quad (6)$$

According to the basic theory of double-beam interference, the intensity of output can be express as

$$I_1 = (E_{r2} + E_{s2})(E_{r2} + E_{s2})^* = I_0 [\varepsilon^2 + (1 - \varepsilon)^2 + 2\varepsilon(1 - \varepsilon) \cos \Delta\varphi] \quad (7)$$

$$\Delta\varphi = k_0(n_s l_s - n_r l_r) - \pi$$

(2) The second phase delay of $\pi/2$ appearing in the reference arm, the probe arm only has the first phase delay.

$$E_{r2}' = A_0 \sqrt{\varepsilon(1 - \varepsilon)} e^{j(\omega t - k_0 n_r l_r + \frac{\pi}{2})} \quad (8)$$

$$E_{s2}' = A_0 \sqrt{\varepsilon(1 - \varepsilon)} e^{j(\omega t - k_0 n_s l_s + \frac{\pi}{2})} \quad (9)$$

$$I_2 = (E_{r2}' + E_{s2}') (E_{r2}' + E_{s2}')^* = I_0 [2\varepsilon(1 - \varepsilon)(1 + \cos \Delta\varphi)] \quad (10)$$

$$\Delta\varphi = k_0(n_s l_s - n_r l_r)$$

where $\Delta\varphi$ is the accumulated phase difference of interference arm.

1.1.1. Theory of the optical fiber inline MZI

The optical fiber inline MZI normally base on the stimulation and coupling of the light waves model that the fundamental mode interferes with the stimulated high-order cladding mode. **Figure 2** schematically illustrates the diagram of optical fiber inline MZI.

The refractive index difference between the fundamental mode (propagating within core) and the m^{th} order cladding mode is

$$\Delta n_{\text{eff}} = n_{\text{eff}}^{\text{core}} - n_{\text{eff}}^{m, \text{clad}} \quad (n_{\text{eff}}^{\text{core}} > n_{\text{eff}}^{m, \text{clad}}) \quad (11)$$

The phase difference of the fundamental mode and the m^{th} order cladding mode can be expressed as

$$\Delta\phi = \frac{2\pi(n_{\text{eff}}^{\text{core}} - n_{\text{eff}}^{m, \text{clad}})L}{\lambda} \quad (12)$$

where $n_{\text{eff}}^{\text{core}}$ and $n_{\text{eff}}^{m, \text{clad}}$ are the effective refractive index of core and m^{th} order cladding mode, accordingly; L is the interference length, that is, the distance between two mode excitation/coupling unit, and λ is the incident wavelength.

The intensity of the interference signal is

$$I = I_{\text{core}} + \sum_m I_{\text{clad}}^m + 2 \sum_m \sqrt{I_{\text{core}} I_{\text{clad}}^m} \cdot \cos(\Delta\phi) \quad (13)$$

where I_{core} and I_{clad}^m are the intensity of fundamental mode and m^{th} order cladding mode, respectively.

Generally speaking, during the experiments, the wave valleys of interference fringes are tracked. The valleys, not peaks are chosen for the comparatively sharper spectrum in experimental

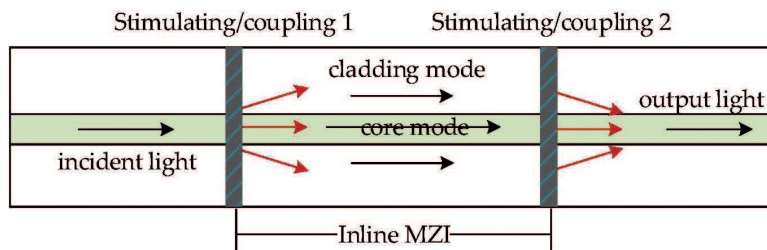


Figure 2. The schematic diagram of optical fiber inline MZI.

results, so that they are more convenient to be tracked. When the phase difference of the fundamental mode and the m^{th} order cladding mode satisfies the condition of destructive interference $\Delta\phi = (2k + 1)\pi$, ($k = 0, 1, 2, \dots$), the wavelength of valley is can be written as

$$\lambda = \frac{2\pi(n_{\text{eff}}^{\text{core}} - n_{\text{eff}}^{\text{m, clad}})L}{(2k + 1)\pi} \quad (14)$$

The wavelength interval of adjacent loss peak is

$$\lambda_{k-1} - \lambda_k = \frac{4\Delta n_{\text{eff}}L}{(2k - 1)(2k + 1)} \quad (15)$$

1.1.2. Principle of fiber temperature sensor based on MZI

According to the theory introduction of optical fiber inline MZI in Section 2.2, the phase difference between the fundamental mode of fiber core and the m^{th} cladding mode is $\Delta\phi = 2\pi\Delta n_{\text{eff}}L/\lambda$. The change of wavelength can be deduced as

$$\Delta\lambda = -\frac{\lambda^2}{\Delta n_{\text{eff}}L} \frac{\Delta(\Delta\phi)}{2\pi} \quad (16)$$

The different materials of fiber core and cladding lead to distinguished thermo-optic properties, relatively, the thermo-optic effect of doped materials is more significant. The thermo-optic effect of optical fiber caused by changeable temperature can lead to the change of the effective refractive difference and length. Thus, the varied phase of optical field induced by temperature can be derived as

$$\frac{d\phi}{dT} = \frac{2\pi}{\lambda} \left(L \frac{dn}{dT} + n \frac{dL}{dT} \right) \quad (17)$$

Furthermore, the variation of phase difference between fundamental mode and m^{th} cladding mode induced by the external temperature change can be written as

$$\begin{aligned} \Delta(\Delta\phi) &= \frac{2\pi}{\lambda} [\Delta n_{\text{eff}}\Delta L + \Delta(\Delta n_{\text{eff}})L] \\ &= \frac{2\pi}{\lambda} \left[\Delta n_{\text{eff}}\alpha L\Delta T + \left(\eta_{\text{co}}n_{\text{eff}}^{\text{core}}\Delta T - \eta_{\text{cl}}n_{\text{eff}}^{\text{m, clad}}\Delta T \right) L \right] \\ &= \frac{2\pi}{\lambda} L\Delta T \left[\Delta n_{\text{eff}}\alpha + \left(\eta_{\text{co}}n_{\text{eff}}^{\text{core}} - \eta_{\text{cl}}n_{\text{eff}}^{\text{m, clad}} \right) \right] \end{aligned} \quad (18)$$

where η_{co} and η_{cl} are respectively the thermal-optic coefficient of fiber core and cladding, α is the thermal expansion coefficient of the sensing material. Based upon the Eq. (16), the wavelength shift caused by changeable temperature can be expressed as

$$\Delta\lambda = -\frac{\lambda^2}{\Delta n_{\text{eff}}L} \frac{\Delta(\Delta\phi)}{2\pi} = -\frac{\lambda^2}{\Delta n_{\text{eff}}L} \frac{1}{2\pi} \frac{2\pi}{\lambda} L\Delta T \left[\Delta n_{\text{eff}}\alpha + \left(\eta_{\text{co}}n_{\text{eff}}^{\text{core}} - \eta_{\text{cl}}n_{\text{eff}}^{\text{m, clad}} \right) \right] \quad (19)$$

$$= -\lambda \Delta T \left[\alpha + \frac{\eta_{\text{co}} n_{\text{eff}}^{\text{core}} - \eta_{\text{cl}} n_{\text{eff}}^{\text{m, clad}}}{\Delta n_{\text{eff}}} \right]$$

Finally, the sensitivity expression of optical fiber temperature sensor can be deduced as

$$\frac{\Delta \lambda}{\Delta T} = -\lambda \left[\alpha + \frac{\eta_{\text{co}} n_{\text{eff}}^{\text{core}} - \eta_{\text{cl}} n_{\text{eff}}^{\text{m, clad}}}{\Delta n_{\text{eff}}} \right] \quad (20)$$

1.2. Fabrication of fiber temperature sensor

1.2.1. Mach-Zehnder interferometer based on taper fiber

When input light comes to the abrupt tapered, the cladding modes are excited by the first abrupt tapered (or up-taper or lateral-offset splicing joint), after traveling a short optical path of SMF, the cladding modes are recoupled back to the fiber core by the second abrupt tapered (or up-taper or lateral-offset splicing joint), they will form interference resulted from the phase difference between the cladding mode and the core mode, as shown in **Figure 3**. The temperature changing will cause the interference fringes movement, thus we obtain the temperature sensitivities by tracking the wavelength shift of interference fringes, which forms the temperature MZI.

In this section, we introduce three types of MZ temperature fiber sensors which include abrupt tapered and up-taper and lateral-offset splicing joint. Due to the advantages of abrupt tapered with simple structure, easy fabrication, many scholars have studied widely. As shown in **Figure 4**. A fiber inline Mach-Zehnder interferometer (MZI) consisting of ultra-abrupt fiber tapers is fabricated [1]. Both the length and diameter of the abrupt tapered are only 100 μm . Temperature sensitivity of the MZI at a length of 30 mm is 0.061 nm/ $^{\circ}\text{C}$ from 30 to 350 $^{\circ}\text{C}$.

An ultrasensitive temperature sensor based on an isopropanol-sealed optical microfiber taper (OMT) in a capillary is proposed [2]. As shown in **Figure 5**, the diameter of the taper is 7.2 μm and the total length L is 2350 μm . The thermo-optic effect and the thermal expansions of isopropanol turn the OMT into an ultrasensitive temperature sensor. The maximum temperature sensitivity of this sensor is -3.88 nm/ $^{\circ}\text{C}$ in the range of 20–50 $^{\circ}\text{C}$.

An in-line MZI sensor with an abrupt tapered is reported [3]. As shown in **Figure 6**. When the temperature changes from 30 to 50 $^{\circ}\text{C}$, the temperature sensitivities of this sensor is 0.0833 dBm/ $^{\circ}\text{C}$ with a standard deviation of 0.27 at 1568.7 nm.

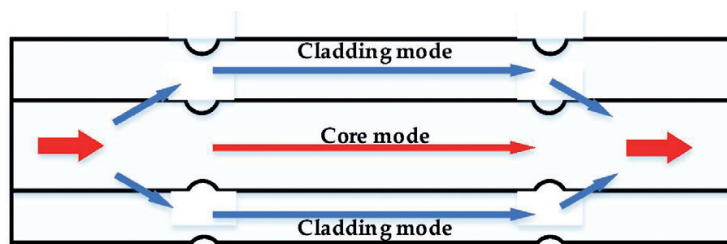


Figure 3. Schematic diagram of MZI.

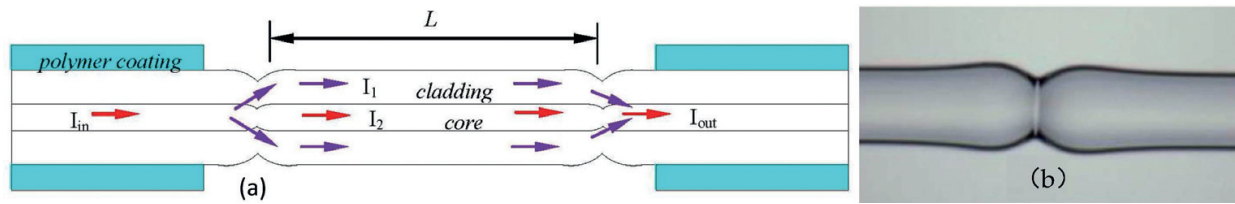


Figure 4. (a) Schematic diagram of the MZI consisting of two ultra-abrupt fiber tapers. (b) The microscopic image of the formed fiber taper.

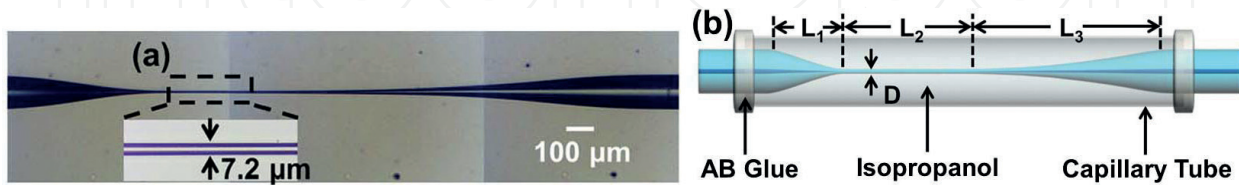


Figure 5. (a) Optical microscope image of the OMT; (b) schematic diagram of the isopropanol-sealed OMT in a capillary.

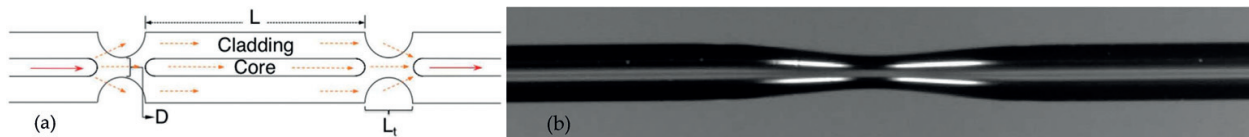


Figure 6. (a) Schematic diagram of an abrupt tapered fiber In-Line MZI; (b) microscopic image of the fabricated abrupt tapered fiber.

In order to increase the robust of the structure, MZI consisting of up-taper has been widely used. **Figure 7** shows the schematic diagram of the fiber-optic MZI which is constructed by two up-taper in SMFs. The diameter and length of the up-taper are 170 and 280 μm , respectively. A high temperature sensitivity of 0.070 $\text{nm}/^\circ\text{C}$ is obtained by a 7.5 mm interferometer [4].

As shown in **Figure 8**, a MZI sensor consisting of a lateral-offset splicing joint and an up-taper is proposed [5]. When the temperature changes from 30 to 110 $^\circ\text{C}$, the temperature sensitivity of MZI is 0.068 $\text{nm}/^\circ\text{C}$ at 1548.41 nm. Two years later, an inline fiber interferometer sensor which consists of a core-offset attenuator and a microsphere-shaped splicing junction is reported [6]. As shown in **Figure 9**. The diameter of microsphere is 250 μm . The temperature sensitivity is 0.0795 $\text{nm}/^\circ\text{C}$ in the range of 200–375 $^\circ\text{C}$.



Figure 7. Configuration of a MZI constructed by two up-taper in SMFs.

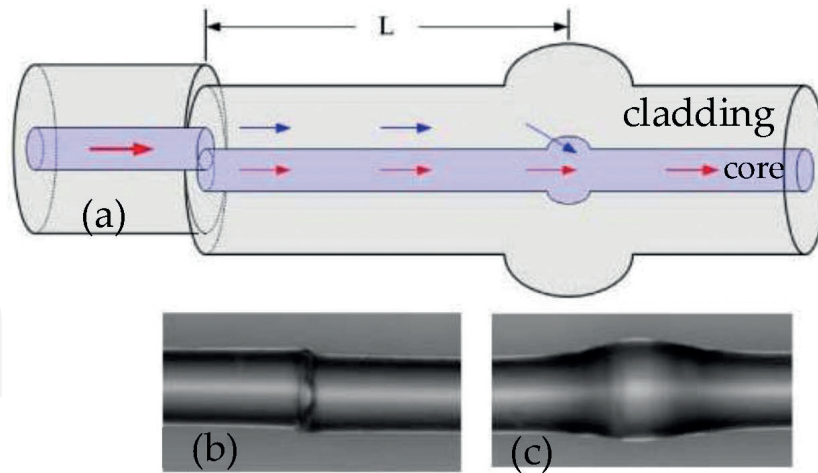


Figure 8. (a) Schematic diagram of the MZI; (b) microscopic image of lateral-offset fusion splicing joint; (c) microscopic image of the up-taper.

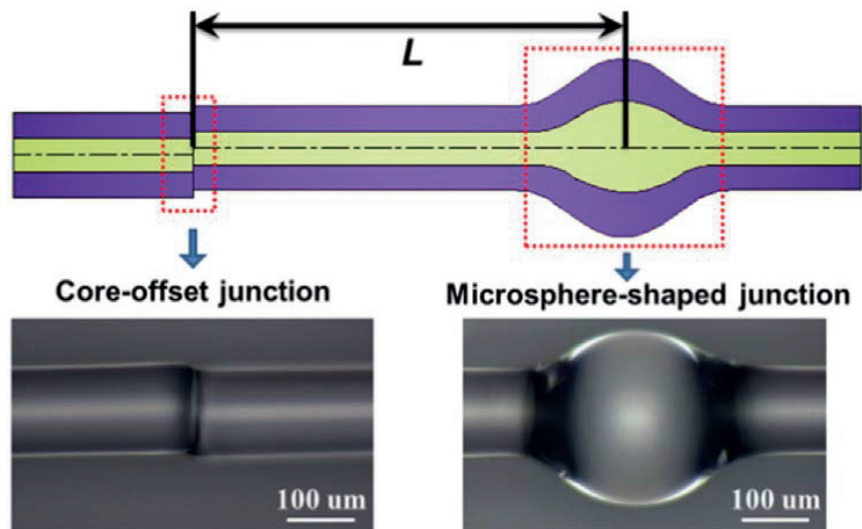


Figure 9. Schematic structure of the interferometer and the optical microscope images of the core-offset and the microsphere-shaped junctions.

1.2.2. Splicing special optical fiber

Using special optical fiber can excite more high code modes to improve sensitivity, therefore, many researchers are attracted to this method. Moreover, the fabrication process is easy by only involving a fusion splicer and fiber cleaver. Based on its potential applications, temperature sensing has been experimentally demonstrated.

A compact and ultrasensitive temperature sensor with a fully liquid-filled photonic crystal fiber (PCF) Mach-Zehnder Interferometer (MZI) was proposed [7]. This temperature sensor consists of a small piece of index-guiding PCF fully infiltrated by fluid and two standard single-mode fibers offset spliced with PCF. The cross-section image of PCF is shown as **Figure 10(a)**. A refractive-index-matching oil (Cargille Labs., $n_0 = 1.38$ at room temperature) is chosen to be filled into the PCF, and its thermo-optic coefficient is $3.56 \times 10^{-4}/\text{K}$. The

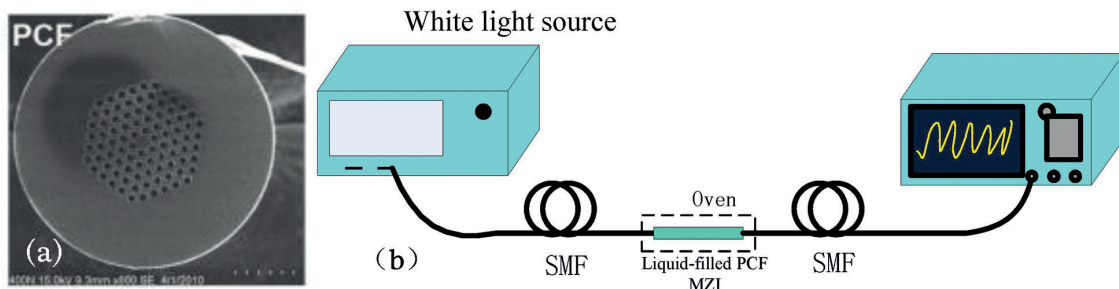


Figure 10. (a) Cross-section of PCF; (b) experimental setup of LF-PCF-based Mach-Zehnder interferometer.

experimental setup is shown as **Figure 10(b)**. The fringes at longer wavelength have higher sensitivity. The temperature sensitivities of the interference dips at 1281 and 1199 nm are $-1.83 \text{ nm}/^\circ\text{C}$ and $-1.09 \text{ nm}/^\circ\text{C}$, respectively. The temperature sensitivity is ultrasensitive, while the temperature sensing part is more compact.

A high-performance temperature sensing using a selectively filled solid-core photonic crystal fiber (PCF) with a central air-bore was demonstrated [8]. The addition of the central air-bore enhances the mode-coupling efficiency between the fundamental core mode and modes in the high index liquid-filled holes in the fiber cladding. **Figure 11(a)** and **(b)** are the scanning electron microscopic (SEM) photos of PCF1. In the fiber model used for simulation (**Figure 11(c)**), a 10-micrometer-thick perfectly matched layer (PML) and scattering boundary conditions are adopted at the periphery of cladding to eliminate boundary reflections. This temperature sensor possesses high sensitivity of $-6.02 \text{ nm}/^\circ\text{C}$, with a resolution of $3.32 \times 10^{-3}^\circ\text{C}$, in the temperature range from -80 to 90°C . This sensor not only improved sensitivity, but also applied the low temperature.

A temperature sensor based on hollow annular core fiber (HACF) was presented [9]. The MZI is consisted by inserting a section of HACF between two sections of multimode fibers. The light beams transmitting along the internal of the HACF. Temperature can be detected through wavelength shift of the interference spectrum. The experimental results show that the temperature sensitivity is up to $30 \text{ pm}/^\circ\text{C}$ in the range of 30 – 100°C . The cross-section photograph of the HACF and schematic diagram of the proposed SMF-HACF-SMF temperature sensor are shown in the inset of **Figure 12(a)** and **(b)**. The interference spectrum of the interferometer is

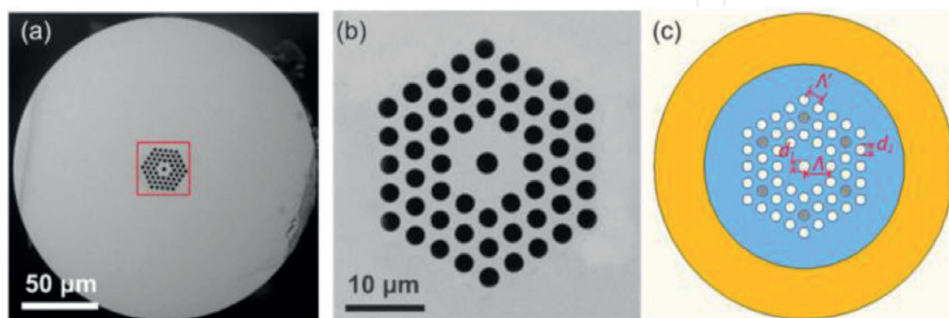


Figure 11. (a) SEM photographs of the fabricated fiber; (b) enlarged cladding area; (c) a simplified model for finite element calculation.

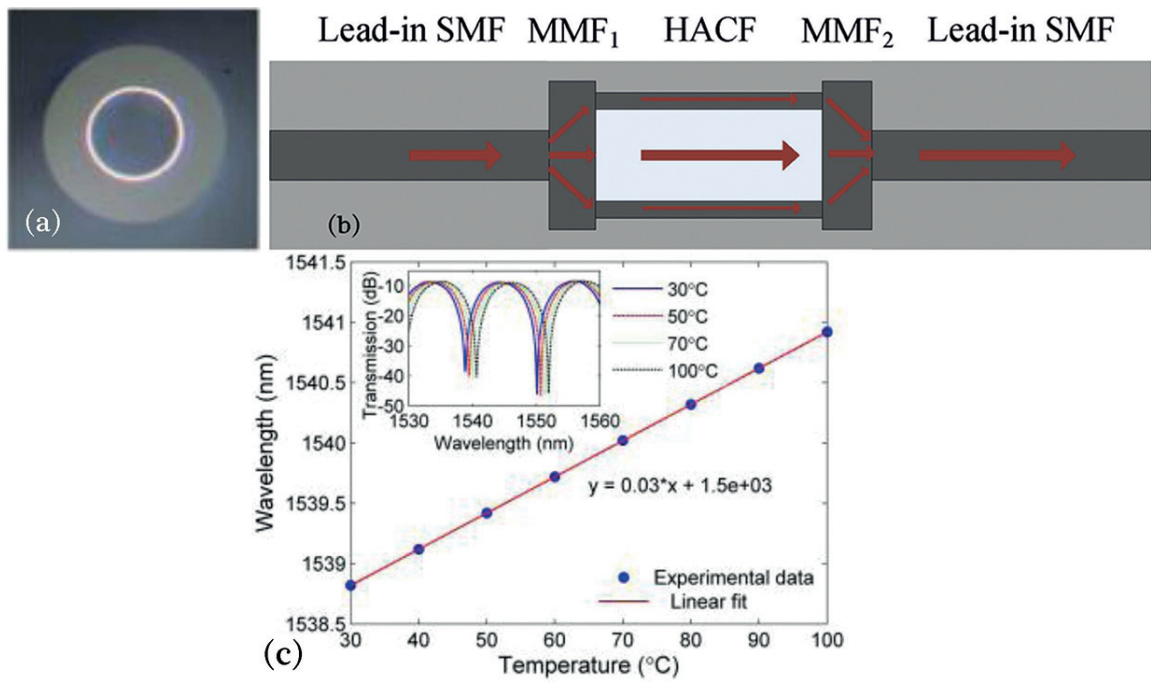


Figure 12. (a) Cross-section photograph of the HACF; (b) schematic diagram of the proposed SMF-HACF-SMF temperature sensor; (c) wavelength shift versus temperature with inset of transmission spectra at different temperature.

shown in the inset of **Figure 12(c)**. From the spectrum, the wavelength separation between two adjacent transmission dips around 1550 nm is 11.4 nm.

The hollow-core-fiber-based interferometer for high-temperature measurements was proposed [10]. They measure temperature up to 900°C with excellent stability and repeatability. The sensing head is comprised of a short hollow-core fiber segment spliced between two single-mode fibers and the offset splicing joint by using a commercial splicer. A high-temperature sensitivity of 41 pm/°C was achieved. **Figure 13(a)** schematically illustrates the structure of the proposed sensor. Temperature response test was performed in a high-temperature oven, which could reach up to 1200°C. **Figure 13(b)** shows experimental device diagram, where a broadband light source (BBS) and optical spectral analyzer was employed to monitor the spectrum.

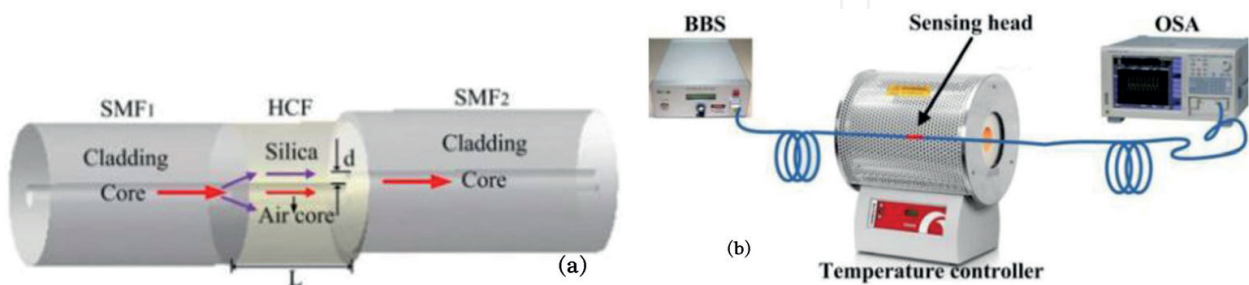


Figure 13. (a) Schematic diagram of the proposed SMF-HCF-SMF temperature sensor; (b) schematic diagram of the experimental setup for temperature tests.

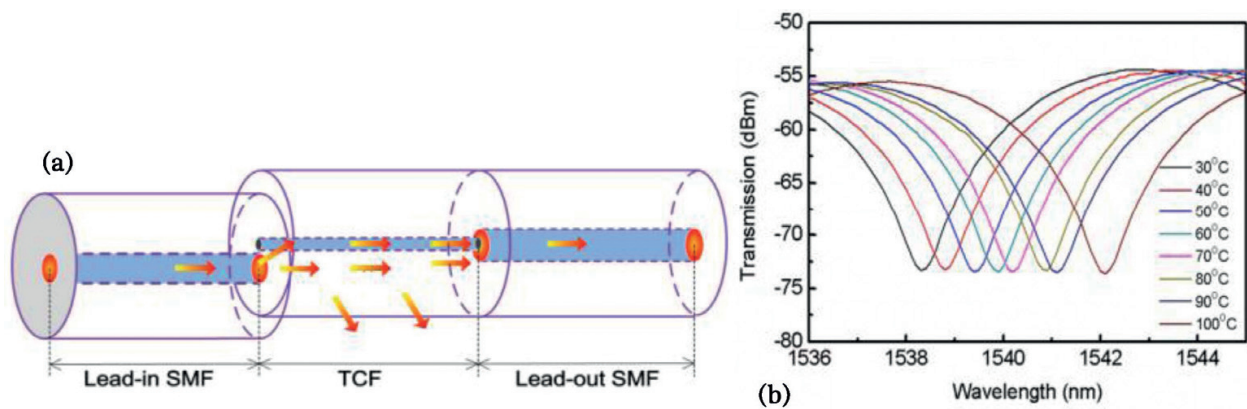


Figure 14. (a) Schematic diagram of the proposed fiber in-line MZI and the propagating light distribution in this structure; (b) interference fringe of the MZI with different temperature.

The fiber MZI temperature sensor, which was fabricated by misaligned splicing a short section of thin core fiber (TCF) between two sections of SMF was proposed [11]. A TCF (Nufern UHNA-3) with a core diameter about 4 μm . This MZI could be used to measure simultaneous of strain and temperature. The temperature was measured with a high sensitivity of 51 pm/ $^{\circ}\text{C}$. **Figure 14(a)** illustrates a 3-D schematic diagram of the proposed fiber in-line MZI structure. Temperature sensor was placing into tube furnace with a temperature range from room temperature to 100 $^{\circ}\text{C}$ with a step of 10 $^{\circ}\text{C}$. As shown in **Figure 14(b)**, interference fringes of the MZI shifted toward a longer wavelength with temperature rise.

A high temperature sensor using multicore fiber (MCF) spliced between two single-mode fibers was proposed [12]. This sensor is simple to fabricate and has been experimentally shown to operate at temperatures up to 1000 $^{\circ}\text{C}$ in a very stable manner. They utilize two core fiber, seven core fiber, 19-core fiber designs through simulation and experiment. Understanding the mode coupling between SMF and MCF allows for the design of devices with sharp spectral features with up to 40 dB resolution for a chosen region of the optical spectrum. At equal coupling, the minima can reach -40 dB for the considered seven-core fiber. A fiber with seven coupled cores supports seven supermodes, shown in **Figure 15(a)**. The 19-core fiber of four supermodes are excited by the fundamental mode of SMF, as shown in **Figure 15(b)**, creating a

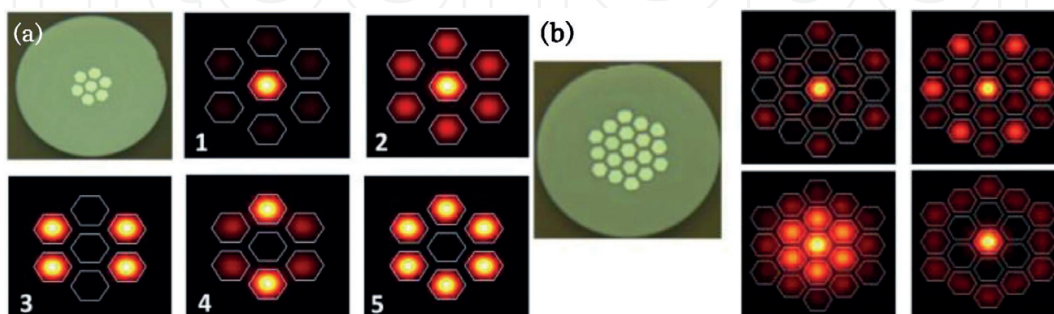


Figure 15. (a) Image of seven-core fiber facet and simulated supermodes supported by the seven-core fiber; (b) image of 19-core fiber facet and simulated supermodes excited by SMF in 19-core fiber.

more complicated interference pattern with more complex periodicity and less sharp spectral features.

In summary, as for the fore-mentioned three types. Temperature sensor is fabricated by special fiber such photonic crystal fiber (PCF), hollow-core-fiber (HCF), thin core fiber (TCF) and multicore fiber (MCF) based MZI. The PCF filling technology improves sensitivity effectively. The other three have advantages of measuring dual-parameters or measure high/low temperature. The cost of splicing type is more affordable, moreover it possesses a higher sensitivity. They could be used for developing a promising microstructure sensor, realizing simultaneous measurement of strain and refractive index and overcoming cross-sensitivity problem.

1.2.3. Femtosecond laser micromachining

Femtosecond lasers present particular advantages in 3D structuring of transparent materials, especially for fiber devices such as compact optical sensors. With femtosecond laser micromachining, the stability and accuracy of microstructure size can be ensured when it is processed. Compared to the open air-cavities fabricated by other methods, the inner air-cavities fabricated by femtosecond laser micromachining has higher robustness.

Figure 16(a) shows a schematic diagram of a miniaturized fiber in-line MZI based on one inner air cavity contiguous to the fiber core for high-temperature sensing. [13] When the incident light reaches the left surface of the air cavity, the core mode turns into the cavity mode and the cladding mode, owing to the abrupt bending imposed by the air cavity. The input light is divided into two parts by the microstructure fabricated on the inner surface of the air cavity, denoted by I_{in1} and I_{in2} , respectively. I_{in1} travels via the air cavity, I_{in2} remains propagating within the fiber core, and interference happens when the two output beams, I_{out1} and I_{out2} , recombine in the fiber core, at the air-cavity end. **Figure 16(b)** shows Interference spectra of the fiber in-line fiber MZI at different temperatures. There is an obvious red shift of fringe dip

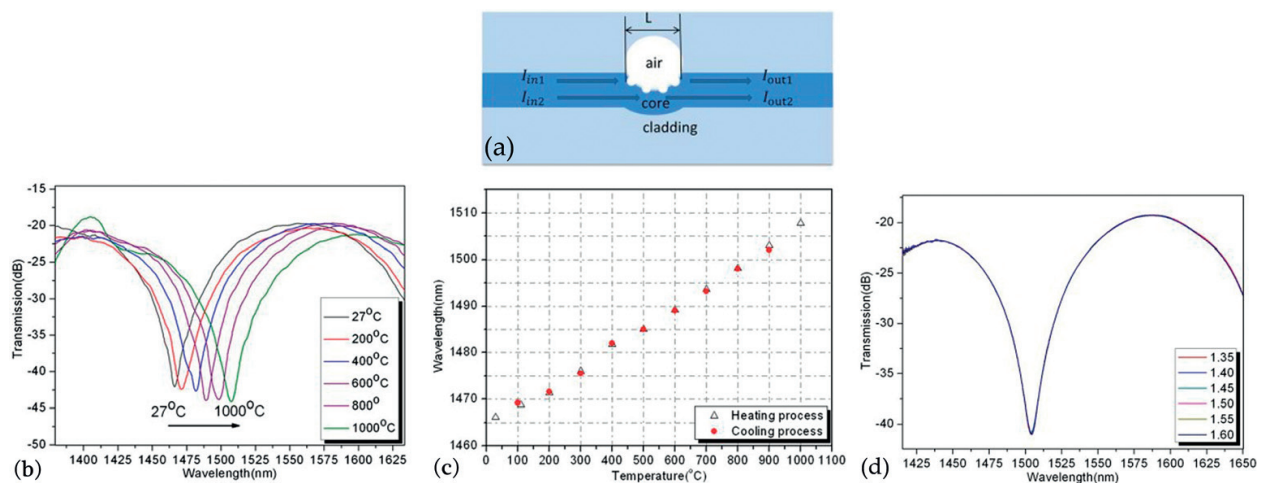


Figure 16. (a) Schematic diagram of fiber in-line MZI. (b) Interference spectra of in-line fiber MZI at different temperatures. (c) Interference dip wavelength versus temperature. (d) Interference spectra of the in-line fiber MZI immersed in different RI liquids.

wavelength as the temperature increases. **Figure 16(c)** shows the relationship between the wavelength shift and the temperature. We can see a good repeatability in both the heating and the cooling processes, and the temperature sensitivity is about 43.2 pm/°C. **Figure 16(d)** shows the transmission spectra of the MZI in different RI liquids. The nearly unchanged spectrum reveals the insensitivity of the device to the surrounding RI. The RI cross sensitivity can be removed by introducing microstructure on the inner surface of the air cavity.

Figure 17(a) shows a schematic diagram of a high-temperature sensor based on a MZI in a conventional single-mode optical fiber, which is fabricated by concatenating two microcavities separated by a middle section, for refractive index and temperature sensing [14]. When the incident light reaches the left surface of the hollow ellipsoid, it is divided into two paths. Part of the incident light is reflected and propagates along path 1. The rest of the incident light propagates across the hollow ellipsoid to the fiber core (path 2), and recombines with the light of path 1. **Figure 17(b)** shows the dip intensity versus curvature. The transmission spectra of the MZI in different NaCl solutions (NaCl solutions are then employed for external RIs measurement with the MZI sensor) are shown in **Figure 2(b)**. The wavelength of attenuation peak A is nearly unchanged in different solutions, indicating the attenuation peak A is nearly insensitive to external RI, which is a desirable merit for temperature sensors because of no cross sensitivity to external RI. The wavelength shifts of peak A with temperature increases is shown in **Figure 17(c)**. The slope of the wavelength shift with temperature in the range of 500–1200°C is 109 pm/°C by linear fitting. The interferometer is especially appropriate for high-temperature sensing because of high sensitivity and good linearity.

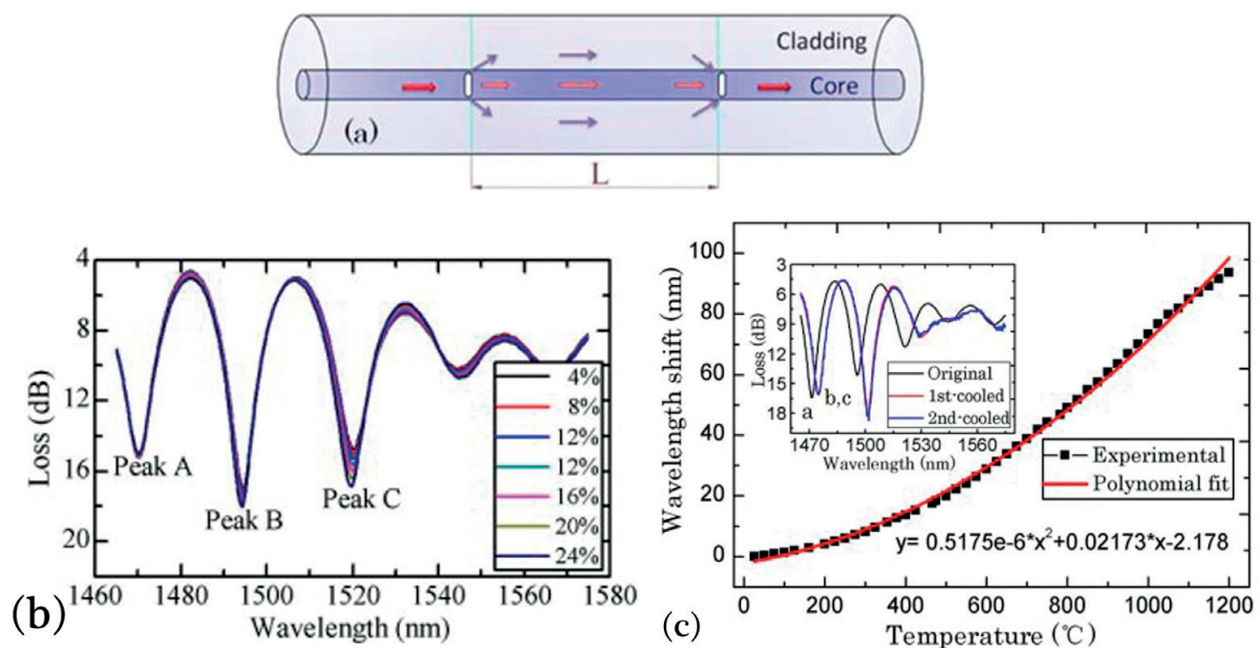


Figure 17. (a) Schematic diagram of the microcavities-based MZI. (b) Transmission spectra of the MZI in different sodium chloride solutions. (c) Wavelength shifts of peak A with temperature increases.

The common characteristic of the two structures mentioned above is that the attenuation peak of the interferometer used for temperature sensing is insensitive to external RIs, which makes the temperature sensor capable of working in a variable refractive index environment without cross sensitivity. However, in many practical applications, it is more and more important for a device to be miniature, robust and can perform a simultaneous multiple parameter measurement sensing in a mutually independent way. **Figure 18(a)** is a schematic diagram of a fiber in-line MZI based on a hollow ellipsoid fabricated by femtosecond laser micromachining and fusion-splicing technique [15]. When the incident light reaches the left surface of the hollow ellipsoid, it is divided into two paths. Part of the incident light is reflected and propagates along path 1. The rest of the incident light propagates across the hollow ellipsoid to the fiber core (path 2), and recombines with the light of path 1 at the right surface of the hollow ellipsoid. **Figure 18(b)** shows the transmission spectrum corresponding to different temperatures, and the slope is $19.4 \text{ pm}/^\circ\text{C}$ by linear fitting in the temperature regions of $24\text{--}1100^\circ\text{C}$. The fringe visibility corresponding to different RI values are displayed in **Figure 18(c)**, where the sensitivity obtained is about -14.3 dB/RIU . **Figure 18(d)** shows the dip intensity versus curvature, and the sensitivity of -0.61 dB/m^{-1} is obtained. Such a device is sensitive to the external RI, curvature, and temperature in an independent manner, which allows a simultaneous measurement of external refractive index, curvature, and high temperature sensing in a mutually independent way. Meanwhile, it is noted that the sensitivity of the device is not high, so it only can be used to measure the high temperature, which has less request for sensitivity.

Simultaneous measurement of the refractive index (RI) and temperature is also of great importance in many biological and chemical applications and environmental monitoring. How to obtain the external temperature and RI at the same time? **Figure 19(a)** is a schematic diagram

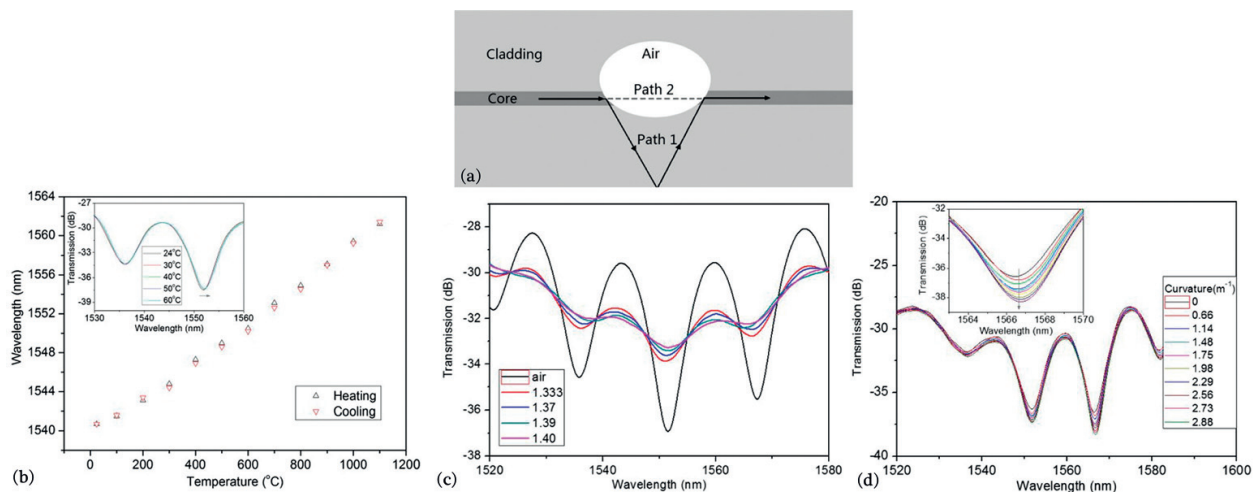


Figure 18. (a) Schematic of the proposed fiber in-line MZI; (b) dip wavelength shift versus temperature; (c) transmission spectra of the device corresponding to different RI values; (d) transmission spectra of the device corresponding to different curvatures.

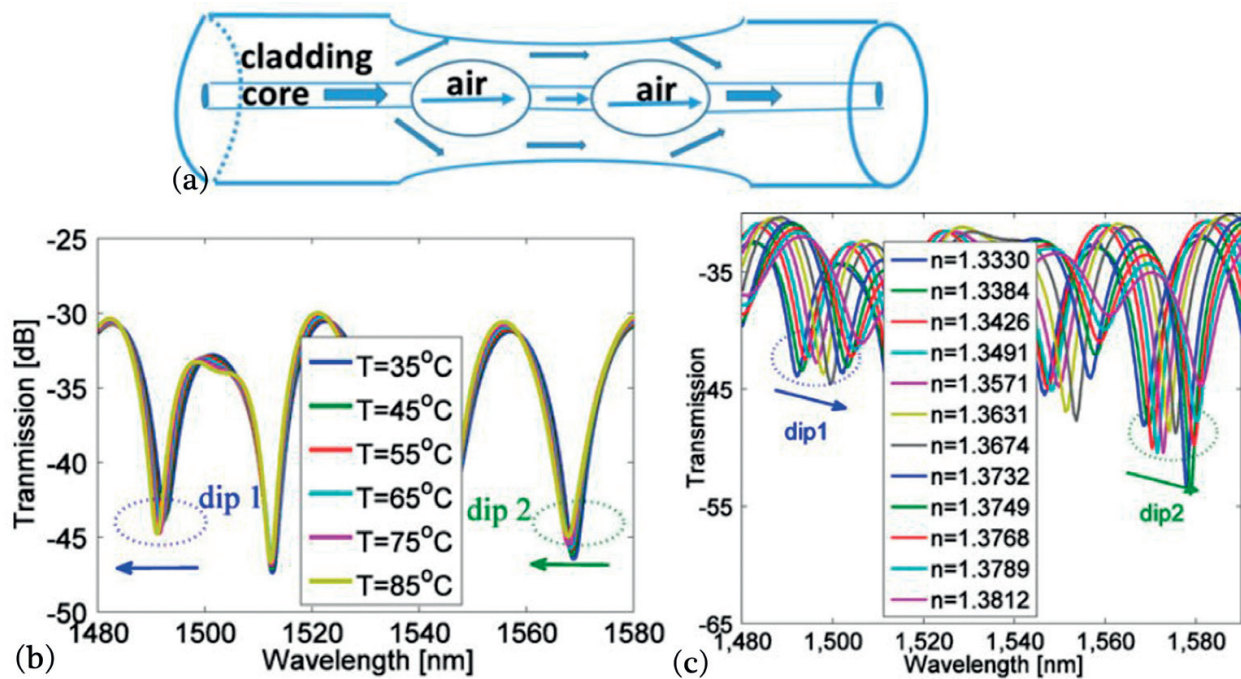


Figure 19. (a) Schematic diagram of the sensing device; (b) transmission spectra of the fiber in-line MZI under different temperatures; (c) transmission spectra of the fiber in-line MZI for different surrounding RIs.

of a fiber in-line MZI based on dual inner air-cavities for simultaneous refractive index and temperature sensing [16]. The dual inner air-cavities are fabricated by use of femtosecond laser micromachining, fusion splicing, and slightly tapering techniques. The input light is split into cladding modes and core modes through the first air-cavity, then the two light beams recombine in the fiber core at the end of the second air-cavity. Using the standard matrix inversion method, the relationship between the shift of dip wavelength and the RI and temperature changes can be written as

$$\begin{bmatrix} \Delta\lambda_1 \\ \Delta\lambda_2 \end{bmatrix} = \begin{bmatrix} k_{T1} & k_{n1} \\ k_{T2} & k_{n2} \end{bmatrix} \begin{bmatrix} \Delta T \\ \Delta n \end{bmatrix} \quad (21)$$

The 2×2 matrix elements can be obtained by the separate measurement of the temperature and the RI responses. Thus the variations in the temperature and RI can be simultaneously determined from the shifts of the two dip wavelengths.

The transmission spectra corresponding to different temperatures and RIs are plotted in **Figure 19(b)** and **(c)**, respectively. In **Figure 19(b)**, the parameters k_{T1} and k_{T2} can be obtained through the two dips of 1493 and 1569. The calculation process is complicated, and the specific derivation can refer to [16]. In **Figure 19(c)**, the parameters k_{n1} and k_{n2} can be figured out in the same method. Thus, it is possible to obtain the change of the temperature and the RI simultaneously while the wavelength shifts of the two dips are determined.

2. Conclusion

In summary, femtosecond laser micromachining is mainly used to fabricate the inner air-cavity structure, which is more robust and miniaturized than that of open air-cavity structure. By choosing different structures, different functions can be realized. The structures of **Figures 16** and **17** have a desirable merit for temperature sensors because of no cross sensitivity to external RI, while simultaneous measurement of the RI and temperature can be realized through the structures of **Figures 18** and **19**.

Acknowledgements

This work is supported by the National Natural Science Foundation of China (NSFC) under Grant Nos. 61078006 and 61275066, and the National Key Technology Research and Development Program of the Ministry of Science and Technology of China under Grants No. 2012BAF14B11.

Author details

Yundong Zhang*, Huaiyin Su, Kai Ma, Fuxing Zhu, Ying Guo and Weiguo Jiang

*Address all correspondence to: ydzhang@hit.edu.cn

National Key Laboratory of Tunable Laser Technology, Institute of Opto-Electronics, Harbin Institute of Technology, Harbin, China

References

- [1] Li B, Jiang L, Wang S, et al. Ultra-abrupt tapered fiber Mach-Zehnder interferometer sensors. *Sensors*. 2011;**11**:5729-5739. DOI: 10.3390/s110605729
- [2] Xue Y, Yong-Sen Y, Yang R. Ultrasensitive temperature sensor based on an isopropanol-sealed optical microfiber taper. *Optics Letters*. 2013;**38**(8):1209-1211. DOI: 10.1364/OL.38.001209
- [3] Raji YM, Lin HS, Ibrahim SA, et al. Intensity-modulated abrupt tapered fiber Mach-Zehnder interferometer for the simultaneous sensing of temperature and curvature. *Optics and Laser Technology*. 2016;**86**:8-13. DOI: 10.1016/j.optlastec.2016.06.006
- [4] Geng Y, Li X, Tan X, et al. High-sensitivity Mach-Zehnder interferometric temperature fiber sensor based on a waist-enlarged fusion bitaper. *IEEE Sensors Journal*. 2011;**11**(11): 2891-2894. DOI: 10.1109/JSEN.2011.2146769

- [5] Zhang S, Zhang W, Gao S. Fiber-optic bending vector sensor based on Mach–Zehnder interferometer exploiting lateral-offset and up-taper. *Optics Letters*. 2012;**37**(21):4480-4482. DOI: 10.1364/OL.37.004480
- [6] Wang M, Jiang L, Wang S. A robust fiber inline interferometer sensor based on a core-offset attenuator and a microsphere-shaped splicing junction. *Optics and Laser Technology*. 2014;**63**:76-82. DOI: 10.1016/j.optlastec.2014.04.002
- [7] Geng Y, Li X, Tan X, et al. Compact and ultrasensitive temperature sensor with a fully liquid-filled photonic crystal fiber Mach–Zehnder interferometer. *IEEE Sensors Journal*. 2013;**14**(1):167-170. DOI: 10.1109/JSEN.2013.2279537
- [8] Ma J, Yu HH, Jiang X, et al. High-performance temperature sensing using a selectively filled solid-core photonic crystal fiber with a central air-bore. *Optics Express*. 2017:25. DOI: 10.1364/OE.25.009406
- [9] Zhang Y, Zhou A, Qin B, et al. Simultaneous measurement of temperature and curvature based on hollow annular core fiber. *Photonics Technology Letters IEEE*. 2014;**26**(11):1128-1131. DOI: 10.1109/LPT.2014.2316532
- [10] Zhang Z, Liao C, Tang J, et al. Hollow-core-fiber-based interferometer for high-temperature measurements. *IEEE Photonics Journal*. 2017;**9**(2):1-9. DOI: 10.1109/JPHOT.2017.2671437
- [11] Zhou J, Liao C, Wang Y, et al. Simultaneous measurement of strain and temperature by employing fiber Mach-Zehnder interferometer. *Optics Express*. 2014;**22**(2):1680. DOI: 10.1364/OE.22.001680
- [12] Van NA, Antoniolopez E, Salcedadelgado G, et al. Optimization of multicore fiber for high-temperature sensing. *Optics Letters*. 2014;**39**(16):4812-4815. DOI: 10.1364/OL.39.004812
- [13] Hu TY, Wang Y, Liao CR, et al. Miniaturized fiber in-line Mach–Zehnder interferometer based on inner air cavity for high-temperature sensing. *Optics Letters*. 2012;**37**:5082-5084. DOI: 10.1364/OL.37.005082
- [14] Jiang L, Yang J, Wang S, et al. Fiber Mach-Zehnder interferometer based on microcavities for high-temperature sensing with high sensitivity. *Optics Letters*. 2011;**36**:3753-3755. DOI: 10.1364/OL.36.003753
- [15] Gong H, Wang DN, Xu B, et al. Miniature and robust optical fiber in-line Mach-Zehnder interferometer based on a hollow ellipsoid. *Optics Letters*. 2015;**40**:3516-3519. DOI: 10.1364/OL.40.003516
- [16] Liu J, Wang DN, Zhang L. Slightly tapered optical fiber with dual inner air-cavities for simultaneous refractive index and temperature measurement. *Journal of Lightwave Technology*. 2016;**34**:4872-4876. DOI: 10.1109/JLT.2016.2590568

